The Scientific Characterization of The PICsIT Detector of the IBIS Telescope

G. Malaguti[a], C. Ciocca[a], G. Di Cocco[a], L. Foschini[a], J.B. Stephen[a], M. Valli[b]

[a]Istituto TESRE/CNR, via Piero Gobetti 101, 40129 Bologna, Italy
[b]ENEA INN-FIS-DIAF, via Don Fiammelli 2, 40129 Bologna, Italy

ABSTRACT

INTEGRAL is the forthcoming European Space Agency's (ESA) satellite mission for gamma-ray astronomy, which will be launched in 2002. IBIS is the imaging telescope onboard INTEGRAL and will produce images of the gamma-ray sky in the region between 15 keV and 10 MeV by means of a two-layer position sensitive detection plane coupled with a coded aperture mask. The detection plane of IBIS comprises two detectors: ISGRI, operative in the 15 keV - 1 MeV range, and PICsIT, 150 keV - 10 MeV. The PICsIT instrument, which is the high energy plane of the IBIS imager, comprises 8 individual modules of 512 detection elements. The modules are arranged in a 4 × 2 pattern, while the pixels are in a 16 × 32 array within each module. Detailed simulation programs of PICsIT qualification and flight model have been set up in order to provide a complete scientific characterization of the detector in terms of spectral and imaging performances. These simulation programs have also been used to reproduce the on-ground calibration results, and will be the basis for the production of the response matrix.

Keywords: Gamma-ray astronomy, gamma-ray detectors, imaging

1. INTRODUCTION AND PICSIT DESIGN OVERVIEW

INTEGRAL[1] (INTErnational Gamma-Ray Astrophysics Laboratory) is the next ESA Medium Size missions for space science within the Horizon 2000 programme and it is due to be launched in October 2002. The scientific objectives of INTEGRAL address imaging and spectroscopy of the high energy sky between few keV and 10 MeV. The satellite payload consists of two main gamma-ray telescopes (one optimised for imaging, and one for spectroscopy), plus two monitors to make simultaneous observations in the X-ray and optical bands.

IBIS[2] (Imager on-Board the INTEGRAL Satellite) is the onboard gamma-ray imaging telescope operating between 15 keV and 10 MeV. In IBIS a coded mask, made of elements opaque and transparent to the incoming radiation, casts a shadow onto a position sensitive detector (PSD) plane that allows the shadowgram to be recorded. When this shadowgram is convolved with the transmission function of the mask, the result is the primary sky image with an accuracy that depends upon the dimension of the mask elements, the mask–PSD distance, and the cross-section of the PSD detection units[3]. The actual detection system of IBIS consists of two arrays of discrete detection units placed one above the other. The top plane, ISGRI[4] (INTEGRAL Soft Gamma-Ray Imager) comprises a 2 mm thick, ~4×4 mm^2 in cross-section 128×128 CdTe elements matrix. At 9.2 mm below ISGRI is placed PICsIT (Pixellated Imaging CsI Telescope). PICsIT consists of a 2×4 modular array. Each modules is a 16×32 matrix of 3 cm thick CsI(Tl) scintillation units. Each CsI(Tl) crystal is ~8.35×8.35 mm^2, physically and optically isolated from the others, and is optically coupled with a photodiode (PD) for scintillation light collection. A passive collimation system is present between ISGRI and the coded mask to shield the detectors against the cosmic diffuse background up to about 300 keV, while an active veto surrounds the sides and bottom of PICsIT. IBIS coded mask is placed at ~3.2 meters above PICsIT and defines a fully coded field of view of 9×9 square degrees. At that distance, one mask pixel, 1.12 cm wide, subtends an angle of ~12 arcmin which defines the angular resolution of the telescope, while the point source location accuracy for strong sources (~20σ) is about 1 arcmin.

PICsIT has been designed to attain with the same instrument good sensitivity, fine imaging, and moderate energy resolution in the low energy gamma-ray domain between 150 keV and 10 MeV.

X-Ray and Gamma-Ray Instrumentation for Astronomy XII, Kathryn A. Flanagan, Oswald H. W. Siegmund, Editors, Proceedings of SPIE Vol. 4497 (2002)

PICsIT key performance characteristics	
Energy Range	150 keV – 10 MeV
Active area	~2856 cm^2
Detection efficiency	~50% at 662 keV
Field of view	9 × 9 square degrees (fully coded) 29 × 29 square degrees (zero response coding)
Angular resolution	12 arcmin
Point source location accuracy	~1 arcmin (~20σ source)
Energy resolution	12% at 662 keV
Time resolution	1 ms (photon-photon and spectral imaging mode)

Table 1. PICsIT scientific performance characteristics

The Qualification Model (QM) of PICsIT, which consists of one 512 pixel module, has been tested and calibrated in 2000, while the Flight Model (FM) will be tested and calibrated in Autumn 2001. In the following sections the scientific characterization of PICsIT is presented and discussed showing simulated results concerning the spectral and imaging capabilities compared with the data obtained during QM ground calibration measurements.

2. PICSIT RESPONSE: LINEARITY, GAIN, ENERGY RESOLUTION, EFFICIENY

The characterization of PICsIT in terms of spectroscopic capabilities has been performed to study the behaviour of the instrument in terms of its key performance parameters both technical (gain, offset, linearity, etc…), and scientific (energy resolution, spatial resolution, event characterization, imaging capabilities, etc…). This has been done coupling and comparing the laboratory results obtained during PICsIT QM calibrations, with simulation data.

2.1. PICSIT MONTECARLO MODELLING

A detailed PICsIT MonteCarlo simulation package, based upon the photon-particle transport code GEANT, has been developed. The simulation consists of two main parts: a) the mass model, which is the actual simulation of the high energy photon and particles interacting with the passive and active materials of a model which represents PICsIT material and geometrical properties, and b) the response model, which contains the detector finite energy resolutions, thresholds, and onboard data handling.

The mass model is an accurate coding of PICsIT active and passive materials, with the possibility to "insert" this in a simplified (in terms of geometry and mass distribution) IBIS model. Within PICsIT, each of the 4096 pixels (or 512 in the case of the QM) has been modeled completely with its diffusive coating, eggcrate housing, and attached Silicon photodiode. Each photon is propagated through PICsIT mass model, by selecting its initial position and trajectory. The photon is then tracked through the simulated set-up, and the implemented interactions include pair production, Compton scattering, and photoelectric absorption. All secondary photons and particles produced are tracked by the programme, and, for each interaction, the energy deposit, the position, and the interaction mechanism are stored.

For each incident photon, all pixels are searched for an energy deposit. The detector energy resolution is then simulated by adding an error, randomly chosen from a gaussian distribution, to the energy deposit in each single pixel (or to the sum of the energy deposits in the case of more than one interaction in the same pixel). The standard deviation of the adopted gaussian is an input parameter determined by the experimental single pixel energy resolution obtained during calibrations. During calibrations only a limited number of energy lines has been used (see section 2.2), and the energy

resolution at all energies has been calculated by means of an empirical fit, which for PICsIT QM was given by the following relation:

$$\left(\frac{\Delta E}{E}\right)_{FWHM} = -0.0078 + 16.8 \times E^{-0.753}$$

where E is the unbroadened energy deposit. After energy resolution spreading, the low energy threshold is applied pixel by pixel.

The data accumulated during the ground calibration campaigns are used to "feed" and validate the MonteCarlo simulation at the energies tested during calibration runs. In fact the photon-particle transport code used for the simulation treats the instrument geometry and interaction physics in great detail. However, the code does not model the response of the detector in terms of linearity, threshold, gain and resolution. After the simulation has been validated at these energies, it could be used to extend the calibration results to all energies and to configurations (incident energy spectra, angle, etc ...) not studied during the calibration activities.

2.2. PICSIT QM CALIBRATIONS

PICsIT QM is a 16×32 (512) pixel module (the final detector is made of 8 of such modules). The experimental set-up was irradiated with radioactive sources placed at 40 cm above the detection plane. Table 2 shows the four sources used during QM calibration which gave a total of six calibration lines, covering the energy interval between 279 and 1836 keV. For four out of the 512 pixels, the PD has been inserted "naked" in order to measure the noise due to the electronic chain.

Radioactive sources and line energies used for PICsIT QM scientific calibration			
Source	**Half life**	**Line energies (keV)**	**Activity (μCi)**
^{137}Cs	30 years	662	10, 100
^{22}Na	2.6 years	511, 1275	10, 100
^{88}Y	106 days	898, 1836	20
^{203}Hg	46 days	279	10

Table 2. The data acquisition for the detector characterization performed during PICsIT QM scientific calibration have been done using 4 radioactive sources for a total of six lines.

A certain degree of in-homogeneity is expected in the scientific response of PICsIT QM pixels with respect to FM. This is due to the fact that the QM has been developed while the manufacturing process of the pixel was still in the optimization phase. Therefore, the QM contains pixels coming from different manufacturing lots which do not have the optimum performance. PICsIT QM is completed by the addition of a Test Equipment (TE) for the acquisition, control, and archive of the calibration and test results, and a Science Console for Quick Look analysis[5].

2.3. DETECTOR CHARACTERIZATION

In the few hundred keV region of the electromagnetic spectrum the intrinsic weakness of the gamma-ray flux coming from cosmic sources with respect to the background (~1:50-100), implies the necessity of long (10^5-10^6 s) observing times. Given these long integration times, the calibration of the detectors must be very accurate in order to minimize the effect of systematic errors. As far as photon interaction with matter is concerned, this is the region where Compton scattering dominates (up to 5-6 MeV), and therefore non-diagonal elements of the response matrix are very significant. In the case of PICsIT, a further complication is given by the presence of a high (4096) number of independent detection units, which implies an unavoidable statistical spread in performances. Moreover, due to limitation in the satellite downlink telemetry, a significant amount of raw data pre-processing needs to be performed onboard. The functioning

and effectiveness of these pre-processing algorithms must then be known with great accuracy. The aim of the scientific characterization of PICsIT is therefore the measurement of the key response parameters of each of the 4096 detection units and of PICsIT as a whole, the evaluation of performance dis-uniformities and possible methods for their equalization/correction. All these effects and parameters will eventually have to be accounted for in the production of the response matrix, and then monitored in orbit during the operative life of INTEGRAL (see section 2.3.2.). As anticipated in section 2.1., this work is performed by coupling the laboratory calibration campaigns with a detailed MonteCarlo simulation programme.

2.3.1. LINEARITY

Detectors non-linearity can be separated in differential and integral non-linearity among the 4096 pixels (512 in the case of the QM). The differential non-linearity, to be ascribed to differences in the channel widths of the analogue-to-digital converters, was already studied during PICsIT Engineering Model (EM) calibrations and was found to be negligible compared to the requirements in terms of spectral resolution[6]. The integral non-linearity has been studied during QM calibration irradiating the detector with four sources for a total of six lines between 279 keV and 1.8 MeV (see Table 2).

Since different multiplicities (see section 3) identify independent events, the channel-to-energy non-linearity of PICsIT QM was investigated separately for single, double, and triple events, and the results are shown in Figure 1. Each point in Figure 1 represents the centroid for each of the spectral lines (see table 2) detected at the various multiplicity orders, averaged on all pixels. The superimposed lines (dotted for single events, dashed for doubles, and dot-dashed for triples), represent simple linear regression fits to these points. PICsIT QM shows an excellent linearity with a correlation coefficient greater than 99% for all multiplicities.

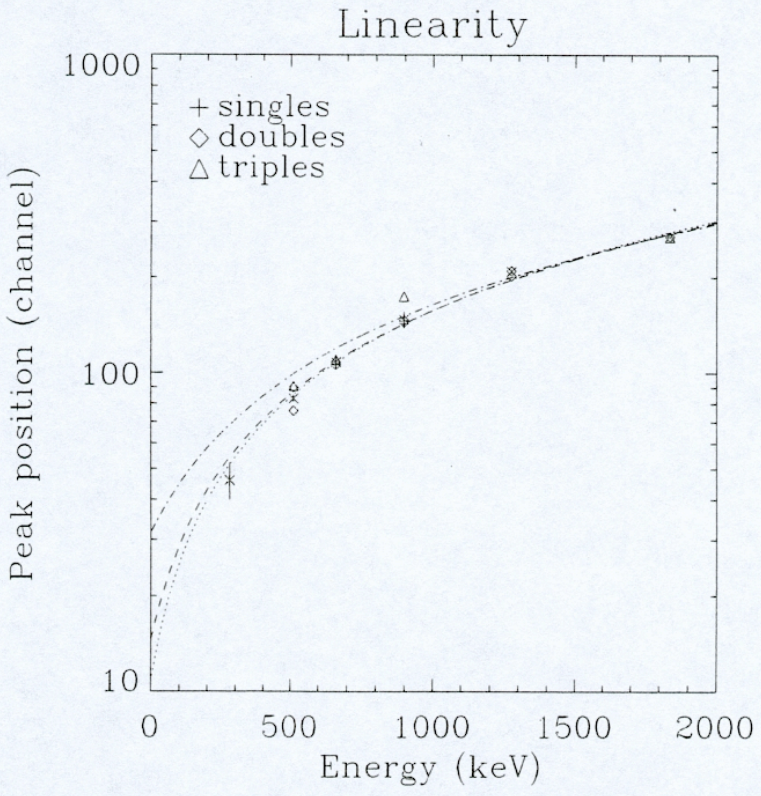

Figure 1: PICsIT channel-to-energy integral linearity for single double and triple events

2.3.2. PIXEL GAIN UNIFORMITY

The channel-to-energy relationship is affected by a number of factors: crystal scintillation efficiency and uniformity, light collection/coupling efficiency, photodiode quantum efficiency, electronic gain, linearity, etc. For simplicity, in what follows we will indicate as *gain* the aggregate result of all these factors. The signal obtained by PICsIT following an energy deposit is converted into the corresponding energy value in keV by means of a look-up table (LUT) which will be available on-board. This LUT contains, for each of the 4096 pixels, a pair of values, gain and offset, which allow the transformation between pulse height channel and energy. The LUT is first obtained during ground calibrations, verified in the commissioning phase, and then monitored during the operative life of the satellite. The expected gain instabilities are due to temperature variations (along the orbit), mechanical shocks (e.g. at the launch), and ageing effects (PD-crystal coupling). A Calibration Unit (CU) is present onboard IBIS which, by means of the emission of tagged 511 and 1275 keV lines, is dedicated to the monitoring (and correction) of the single pixel gain.

The gain of each PICsIT QM pixel was obtained with a simple linear regression fit using the six energy lines (see table 2) available during QM calibrations. Figure 2 shows the distribution of measured gains. The distribution is well fitted by a gaussian curve centered at 6.11±0.21 keV/ch.

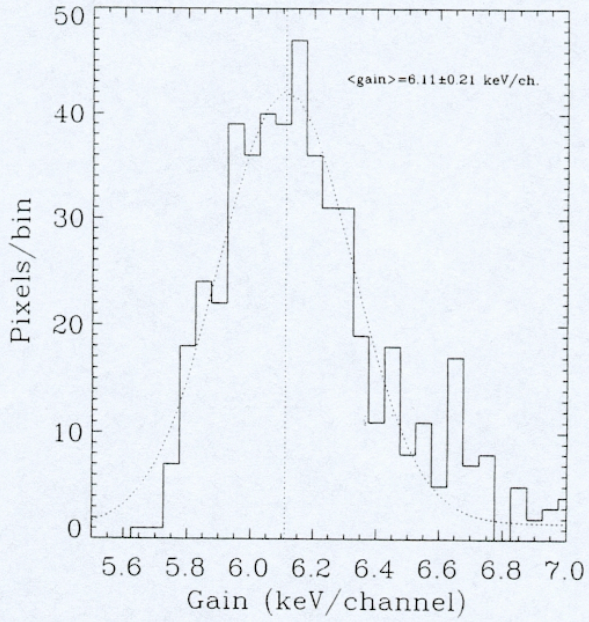

Figure 2: Gain distribution across PICsIT QM detection plane.

As anticipated in section 2.2, and confirmed by the distribution shown in figure 2, the observed pixel gain spread profile is expected. The main reasons for it are to be ascribed to the inhomogeneity in the gain of the ASIC channels, light output distribution in the pixels, and also in the different manufacturing procedures of the QM pixels. In fact QM pixels come from lots which were realized while the optimization of the pixel manufacturing process was still ongoing. This in-homogeneity, however, is a worst case scenario for testing the equalization and correction algorithm which will be run onboard. Even with such a gain in-homogeneity, in fact, once the gain-offset look-up table is obtained for all pixels, it is possible to equalize and correct the raw spectra in a way that simulates what will be done onboard.

Figure 3 shows the effect of such a correction in the case of an ^{88}Y radioactive source which has two lines (898, and 1836 keV). The upper panel of figure 3 shows the superimposed 512 QM raw spectra, with the pulse height expressed in channels, before correction and equalization. After the gain-offset correction LUT is applied, the spectra are

equalized and transformed into keV as shown in the lower panel. This process is part of the event handling software and will be run onboard IBIS. In the case of single events, a further refinement will be possible onground.

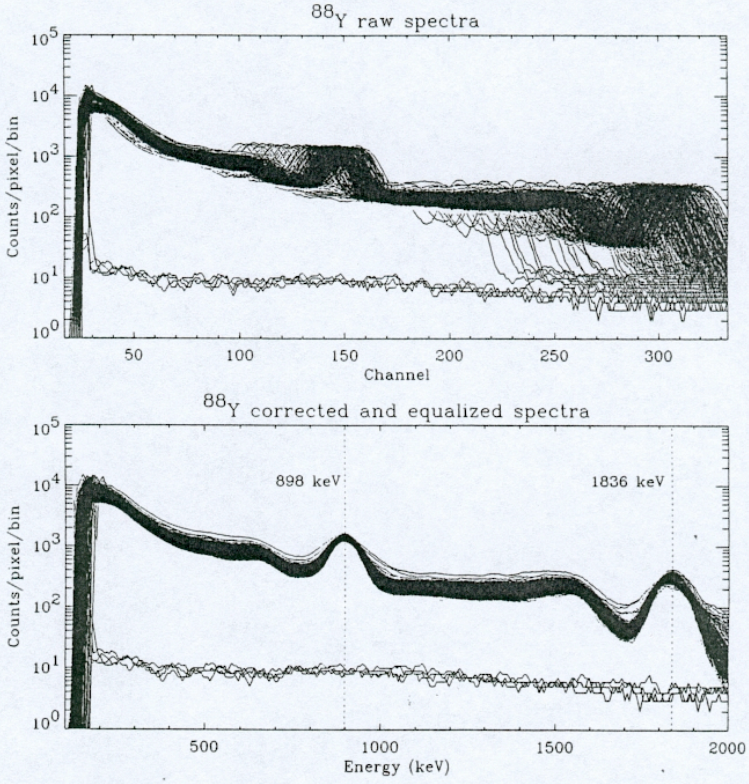

Figure 3: Raw spectra equalization and correction for a ^{88}Y source acquisition.

The four spectra which remain at a level of ~10 counts/second also in the bottom panel of Figure 4 corresponds to the 4 pixels of the QM which have been inserted without the crystal (i.e. the naked photodiode) in order to have a measurement of the electronic noise.

2.3.3. ENERGY RESOLUTION

The theoretical energy resolution of a single PICsIT pixel can be expressed by the noise to signal ratio, which, assuming a Poisson statistics, is given by the following equation:

$$\left(\frac{\Delta E}{E}\right)_{FWHM} = 2.35 \times \frac{\sqrt{n_e \times E_{keV} + Noise^2}}{n_e \times E_{keV}} + K$$

where n_e is the light output in e^-/keV at the photodiode, E_{keV} is the energy deposit in keV, the *Noise* is expressed in electrons rms, and K is the additive factor accounting for scintillation light production and collection in-homogeneities due to crystal non-uniformity. A complete assessment of PICsIT energy resolution capabilities as a function of energy was performed comparing the expected theoretical values with MonteCarlo simulation results and experimental data. The values of n_e and *Noise* are calculated for each pixel during their calibration prior to the insertion in the module. The uncertainty in the knowledge of K, however, determines the impossibility to implement the above equation in the simulation, which instead makes use of a relation obtained from an empirical fit to laboratory data as explained in section 2.1.

The left panel of figure 4 shows the comparison between experimental data (points) obtained during QM calibration and simulation results (dashed and dotted lines) with the theoretical single pixel resolution (continuous line) calculated for n_e=32 e$^-$/keV, *Noise*=950 e$^-$, and K=1.3. A typical error bar due to statistical fitting is also shown for the experimental data. The agreement between MonteCarlo and experimental data is within 5%. The disagreement between the theoretical profile and the single events resolution at low energies is not well understood and suggests an energy dependence of the K factor.

The right panel of figure 4 shows the single pixel energy resolution at 662 keV measured during QM calibrations. The observed gaussian spread is centered at 11.8% with a spread (1σ) of 0.81.

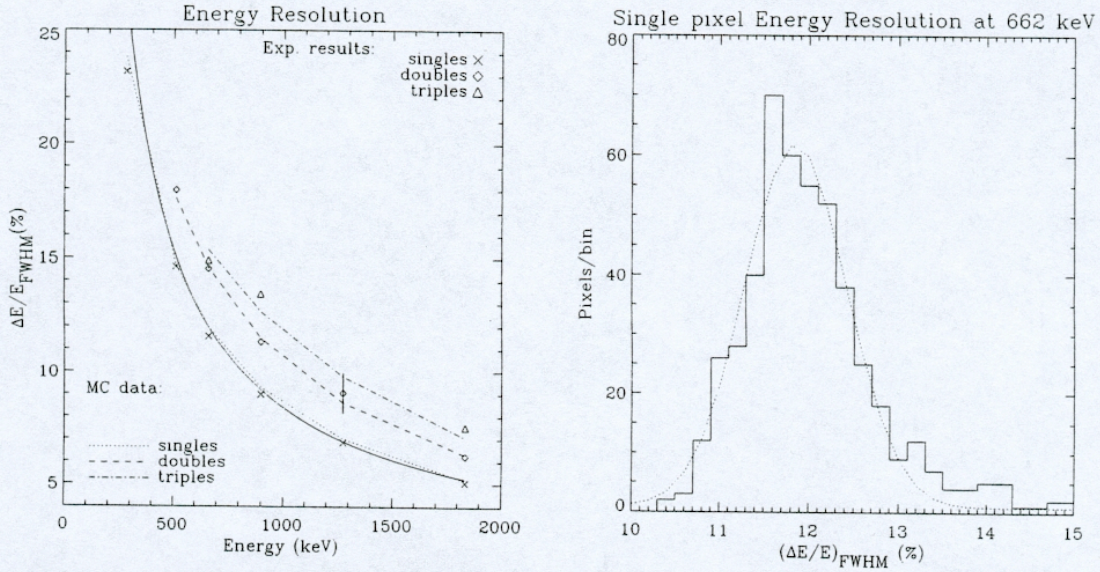

Figure 4: Left panel: Energy resolution profile vs energy for single, double, and triple events: comparison between MonteCarlo (dotted, dashed, and dot-dashed line) and experimental results (data points). The continuous line indicates the expected theoretical values (see text). Right panel: Single events energy resolution measured at 662 keV for all QM pixels.

2.3.4. DETECTION EFFICIENCY

PICsIT detection efficiency has been calculated at the line energies available in the laboratory (see Table 2). The photopeak effective area profile of PICsIT is shown in figure 5. The lines in figure 5 indicate the effective area profile evaluated with the MonteCarlo simulation for the various multiplicities (single, double, and triple events). The superimposed data points have been obtained from calibrations tests on the QM, normalized for the sources activity, and scaled to the complete geometry of PICsIT.

3. EVENT MULTIPLICITY, EDGE EFFECTS, AND ADJACENCY

PICsIT is a pixellated detector. This means that an incident gamma-ray photon can, depending upon its energy, interact in more than one pixel. In order to quantify this effect, the concept of multiplicity has been introduced. One *event* is the sum of all *good* (within the lower and upper energy threshold limit window) energy deposits caused by a incoming gamma-ray photon.

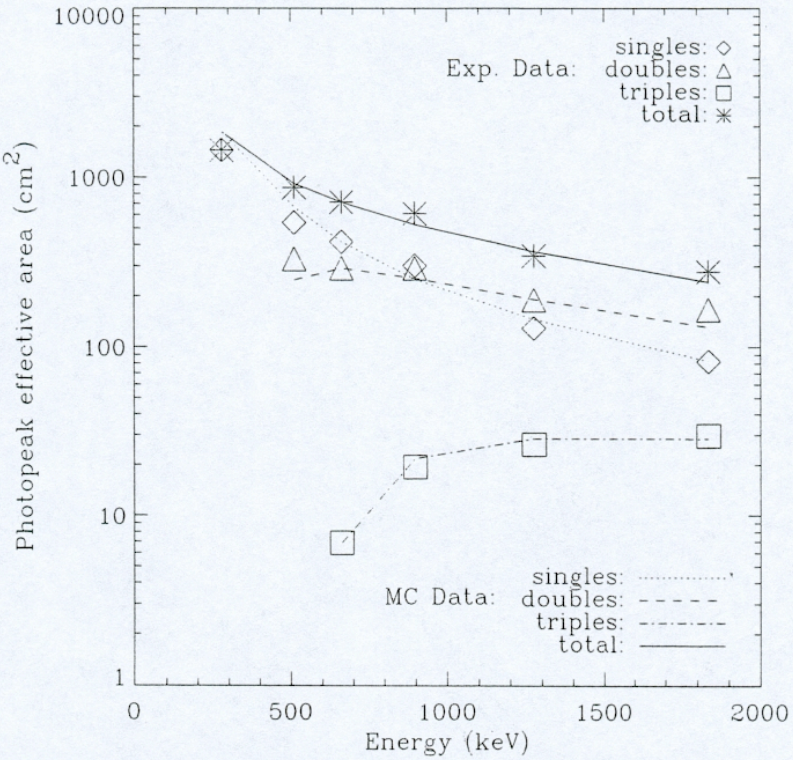

Figure 5: PICsIT photopeak effective area vs energy for different multiplicities: MC results (lines) and experimental data obtained during QM calibrations (points: normalized to the entire PICsIT area). Experimental points contain 1σ error bars.

The *multiplicity* of an event is the number of pixels triggered by the event. The modular nature of PICsIT together with the presence of passive material implies a certain degree of spatial anisotropy in the distribution of events across the detection planes which varies as a function of multiplicity and incident energy. These physical factors are further complicated by the presence of an electronic subdivision inside the modules: each of the 8 modules is electronically separated into two 16×16 semi-module. Therefore a multiple event which triggers pixels in two semi-modules belonging to the same module is seen by PICsIT as two events, each event having the multiplicity registered in each semi-module.

All these effects have been implemented in the simulation. Figure 6 shows the PICsIT QM simulated count maps obtained for single (first column), double (second column) and triple events (third column). All profiles were obtained with a monochromatic incident photon beam of 279 keV (upper panel), 662 keV(middle panel), and 1836 keV (lower panel) placed at a distance of 40 cm. The resulting spatial anisotropies observed in the count maps are expected. Towards the edge of the detector, in fact, the escape probability of an interacting photon is increasing, and therefore multiple events are more likely in the central regions, while single events are more likely in the peripheral ones. The overall result is that single event maps are concave, while multiple event ones are convex.

As can be seen from the upper panel in figure 6 the count map at 279 keV is anomalous with respect to this behaviour. The concave shape is absent since, at this energy, the importance of multiple events is negligible. The observed convex shape, on the other hand, is caused by the solid angle subtended by the simulated source projected onto PICsIT QM detection plane. This effect is amplified by the fact that photons interacting at the periphery "see" a reduced CsI thickness which implies a decrease in the detection efficiency towards the edge of the detector.

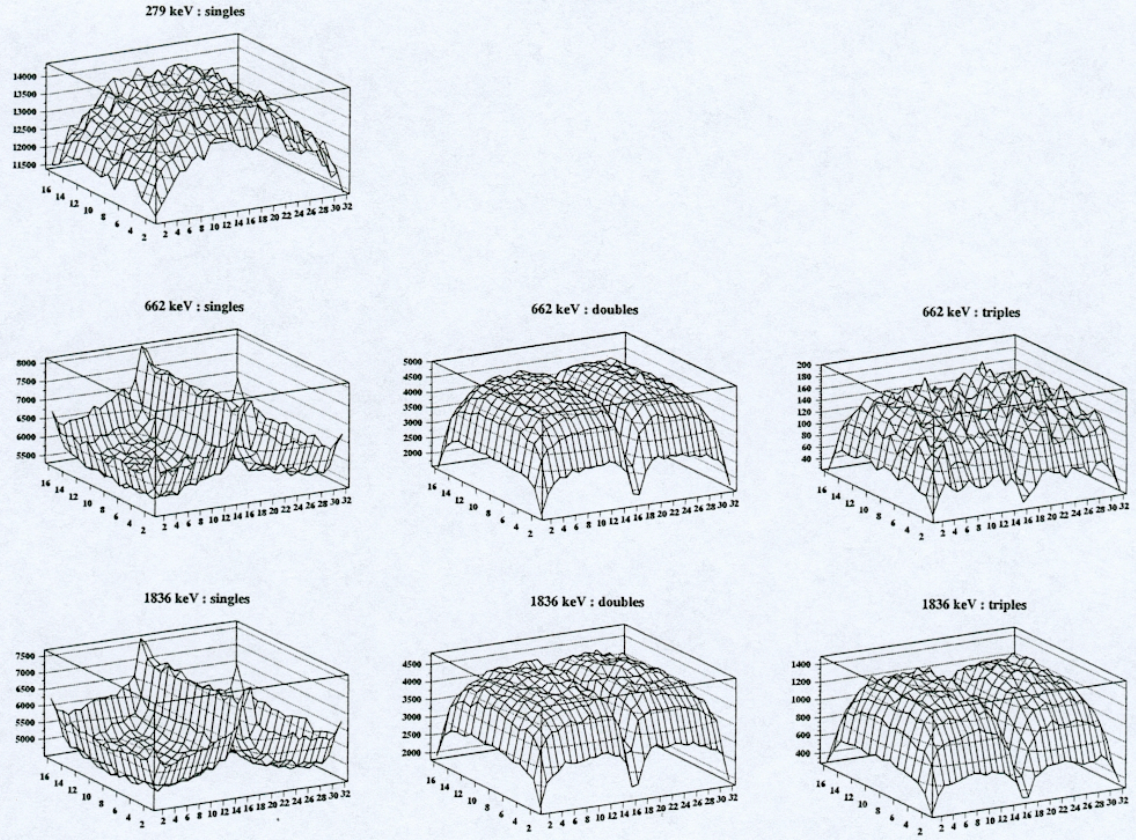

Figure 6. Simulated count maps for PICsIT QM. Single (left column), double (middle column), and triple (right column) events are shown for different incident photon energies: 279 keV (upper line), 662 keV (middle line), and 1836 keV (bottom line).

The spatial anisotropies shown in figure 6 are therefore energy dependent, and have different profile for different multiplicities. This will results in a complex profile of the background which will have to be accounted for in the production of the response matrix. It is important to point out, however, that in the final flight configuration, the presence of an anticoincidence active shield around PICsIT will mitigate these anisotropies by detecting a large percentage of the escaping photons which have interacted in PICsIT.

3.1. MULTIPLE EVENTS HANDLING

For the formation of the shadowgram, i.e. the count map produced by the source illumination modulated by the coded mask, each event is assigned to a single pixel. In the case of single events this is trivial. Multiple events, on the other hand, have to be pre-processed onboard for satellite telemetry limitation and one reconstructed incidence pixel (and one energy value) is associated to them. In this way multiple events can be described with the same amount of telemetry resources as single events, and are put in a dedicated downlink datastream. The reconstruction algorithm is part of IBIS

onboard software and its accuracy depends on the total energy deposit of the event, while the magnitude of the error (in detector pixel) depends on the adjacency order of the multiple event.

3.1.1. INCIDENT PIXEL RECONSTRUCTION ACCURACY

The method envisaged for onboard reconstruction of the incidence pixels of PICsIT multiple events is based upon their total energy deposits. For a total energy deposit $E_{tot}<E^*$, the event is assigned to the pixel having the lower energy deposit, while for $E_{tot}>E^*$ it is assigned to the pixel having the higher energy deposit. The value of E^* is determined by MonteCarlo simulation coupled to ground calibration, and is in any case an IBIS onboard parameter that can be changed via telecommand. Table 3 shows the efficiency of the incidence pixel reconstruction for double and triple events.

	Events (%) for which the Min (Max) energy deposit has been released in the incidence pixel				
Incident Energy	**Double events**		**Triple events**		
	Min	Max	Min	Mid	Max
279 keV	45.2	37.6	--	--	--
511 keV	38.7	40.0	31.0	28.5	27.5
662 keV	29.4	48.4	25.6	27.8	36.1
898 keV	20.2	57.6	17.4	23.6	47.5
1275 keV	15.4	61.9	10.9	19.7	56.2
1836 keV	12.8	64.4	7.3	15.3	62.5

Table 3. Incidence pixel reconstruction accuracy as a function of energy for double (columns 2,3) and triple events (columns 4,5,6).

Table 3 shows that with such a simple algorithm it is possible to reconstruct the correct incidence pixel for a fraction of PICsIT multiple events that varies between ~40% at 511 keV to ~64% at 1.8 MeV.

3.1.2. ADJACENCY ORDER

When the above method described for incidence pixel reconstruction does fail, the event is assigned to the wrong pixel. As far as the shadowgram coupling with the coded mask is concerned, it is important to have an evaluation of the magnitude of this error, i.e. the distance between the (wrongly) reconstructed pixel, and the real incidence pixel. This distance varies upon the total energy of the multiple event, but depends also on the *adjacency order* of the event. The adjacency order is defined as the (maximum, in the case of triple events) distance, expressed in units of pixel pitch (which for PICsIT amounts to 0.92 cm), between the triggered pixels. The adjacency can therefore be assimilated to the point spread function for multiple events in the case of a pixellated detector.

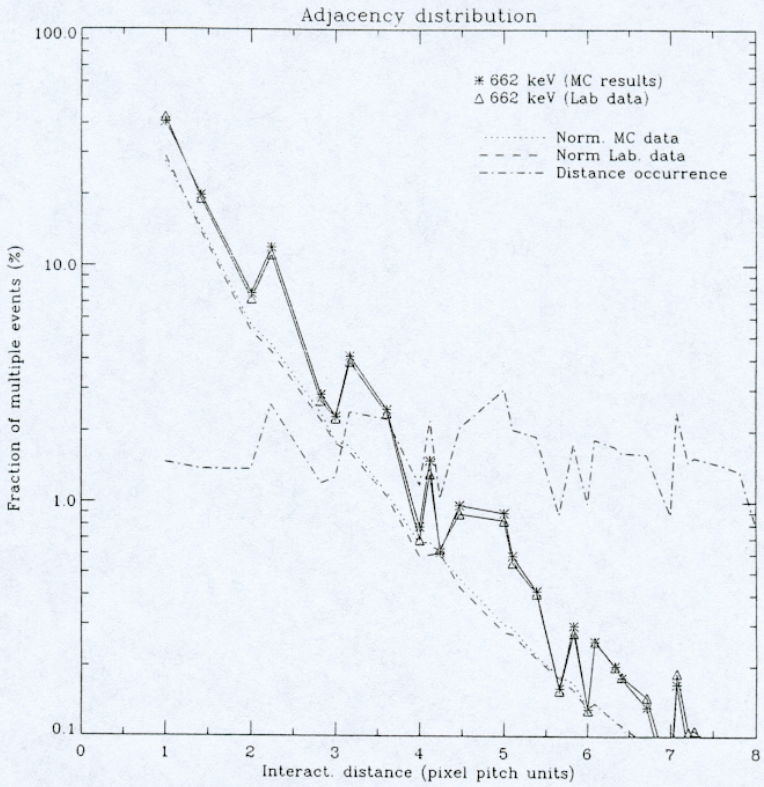

Figure 7. PICsIT experimental (triangles) and simulated (stars) multiple events adjacency order profiles (continuous lines). The dotted (MC data) and dashed (lab data) lines represent the same adjacency profiles normalized for the occurrences of each possible distance (dash-dotted line) due to simple geometrical effects.

Figure 7 shows the experimental (triangles) and simulated (stars) PICsIT QM adjacency profiles for multiple events in the case of a ^{137}Cs source. The agreement between laboratory and MonteCarlo results is very satisfactory. The discontinuities observed in both profiles are due to the geometrical finiteness of the PICsIT QM module. If the observed (MonteCarlo and experimental) adjacency orders profiles are divided by the respective geometrical occurrences (dash-dotted line in figure 7) the smooth (dotted and dashed) lines are obtained.

4. PICSIT IMAGING CAPABILITIES

In order to test both the PICsIT imaging capabilities, and the effectiveness of the deconvolution algorithms, the detailed mass model of PICsIT has been coupled with a simplified simulation of IBIS which included the coded mask. The shadowgram has been obtained by simulating the galactic center region containing the two sources SGR X-1 and GX359+02.

The images were deconvolved using the traditional 'balanced correlation' technique[3] for coded aperture instruments. This consists of a cross-correlation between the data and a deconvolution array derived from the mask pattern, in this case rebinned to the same spatial dimensions as the detector array. In order to fully exploit the wide field of view of the instrument it is necessary to create an image not just for sources in the fully coded field of view, but also for those which are vignetted, or partially coded – which accounts for most of the field of view, albeit at a lower sensitivity. In order to make the images as uniform as possible, and remembering that background counts dominate the images, the

deconvolution can be performed by using a weighting array which takes into account the effective exposure of each detector pixel for every sky position.

An effective image analysis and reconstruction must identify each source, reconstruct which of the possible multiple positions is consistent with the data and remove the other instances of the same source (also correcting for systematic background variations due to the source). This is performed in an iterative manner, starting from the strongest source. As can be seen for the image shown in figure 8, this is capable of producing an image which is quite uniform, but with multiple instances of the same source, one in the fully coded field of view and several others corresponding to possible vignetted positions of the same source.

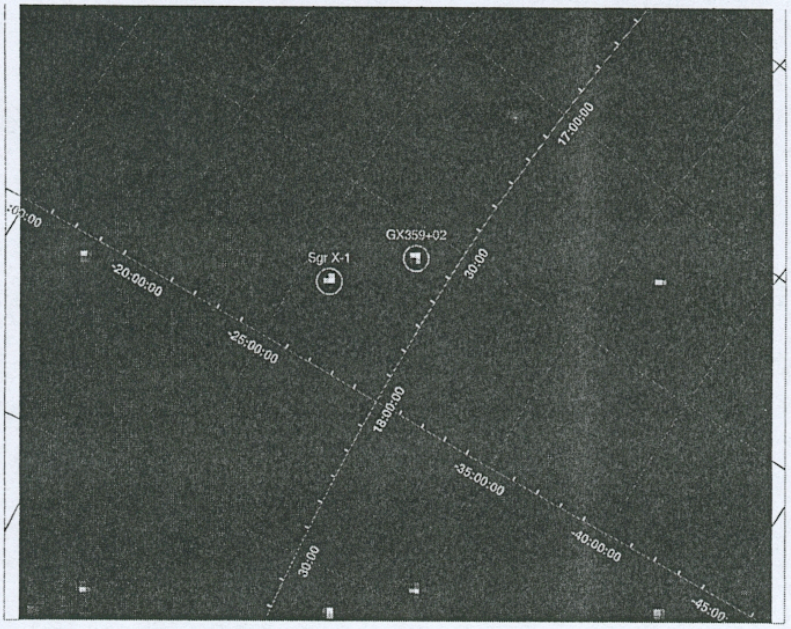

Figure 8. PICsIT simulated image of the Galactic Centre region (one pixel corresponds to 12 arcminutes).

5. REFERENCES

1. 1. C. Winkler, "INTEGRAL: the current status", Proc. of 3rd INTEGRAL Workshop The Extreme Universe, Taormina, Sept. 1998,
2. P. Ubertini et al., "The IBIS Gamma-Ray Telescope on INTEGRAL", Proc. of the 5th Compton Symposium, AIP, 2000. M. L. McConnell and J. M. Ryan eds., 510., p.684
3. E. Caroli et al. 1987, "Coded aperture imaging in gamma-ray astronomy", *Spa. Sci. Rev.*, **45**, p. 349
4. F. Lebrun et al., "A CdTe gamma-camera for the space observatory INTEGRAL", *Nucl. Instr. & Meth.*, **A380**, p. 414
5. M. Trifoglio et al. 1999, "Science test equipment for the INTEGRAL PICsIT instrument", SPIE Proc., Vol. 3765, p. 572
6. G. Malaguti, G. Di Cocco, and J.B. Stephen, 1999, "Scientific calibration of the PICsIT engineering model detector of the IBIS telescope", SPIE Proc., Vol. 3765, p. 33